Vertical Upward Flow Patterns in Small Diameter Tubes

L. Chen* **Y. S. Tian**** **and** **T. G. Karayiannis****

* Department of Engineering Systems, London South Bank University, 103 Borough Road, London SE1 0AA, U.K., E-mail: tassos.karayiannis@lsbu.ac.uk
** Aspentech Inc., The Gemini Building, Fermi Avenue, Didcot, Oxfordshire, OX11 9QR, U.K.

ABSTRACT

Two-phase flow patterns were studied in vertical small diameter tubes using R134a as the working fluid. The observed flow patterns include bubbly, dispersed bubble, confined bubble, slug, churn, annular and mist flow. Twelve flow pattern maps, derived from four internal diameters (1.10, 2.01, 2.88 and 4.26 mm) and three different pressures (6, 10, 14 bar), are presented. The flow patterns exhibit strong "small tube characteristics" described in earlier studies when the tube diameter is 2 mm or less. Slug-churn and churn-annular boundaries depend on diameter and pressure. Dispersed bubble-churn and bubbly-slug are less affected. The transition boundaries are compared with existing models for normal size tubes showing poor agreement. Various coordinate systems were considered for the flow maps. The results show that the Lockhard-Martinelli Parameter and mass flow flux can account for the effect of fluid pressure on flow patterns.

Keywords: Two-phase flow patterns, small diameter tubes

INTRODUCTION

The study of two-phase flow regimes in small channels is an important current research topic; firstly, it plays an important role in modern industries [1-3] and secondly, the flow pattern transition mechanisms are quite vague and disputable although some common characteristics exhibited in small tubes have been recognized by various researchers [4-6]. Thus, there are a number of arguments among different researchers, which need further experimental work and theoretical investigation.

The definition of small or micro tubes has not been generally agreed, which makes the comparisons between the experiments difficult, especially when using different fluid or at different experimental conditions. In general, tubes of diameter in the order of centimetre and millimetre are regarded as normal (traditional) and small tubes respectively. Recently, many researchers argued that the criterion ought to be based on thermo-hydraulic properties rather than only on channel dimension. Fukano and Kariyasaki [1] experimentally investigated the effect of diameter using air-water flow in 1 to 9 mm tubes at atmospheric conditions. They found the critical diameter, at which the surface tension surpasses the gravity, is between 5 to 9 mm and the effect of diameter dominated over flow direction when the tube diameters were smaller than 6 mm. The conclusions agreed with the criterion of Kew and Cornwell [7]. They found that two-phase flow exhibits different flow and heat transfer characteristics when the confined number Co>0.5. This depends on the diameter as well as surface tension and density (pressure) of the liquid and vapour. Brauner and Moalem-Maron [8] thought the surface tension dominates other forces when Eotvös number $E\ddot{o} > 1$. Triplett et al. [9] reported that the stratified flow vanished as $E\ddot{o} > 100$. All above three criteria represent flow characteristics in small channels. However, the discrepancy is quite significant, see also [10].

The classification of flow patterns in small channels is not as yet generally agreed. In fact, flow maps sketched by different researchers may be dissimilar even though they use similar tubes

*Corresponding author

Reported results can hardly be ere is no accepted benchmark result. In fact the factors affecting flow patterns are numerous and complex. Also the identification of flow patterns is greatly affected by the observer's subjectivity and the experimental technique employed. The transition from one flow pattern to another may be abrupt but in most cases it is a gradual development process in which case the transition boundary becomes a transition zone. Within the transition zones the flow patterns possess characteristics of more than one of the flow patterns. The above factors constitute the main causation leading to the lack of clarity. However, although there are arguments on the classification of the flow patterns, most researchers agreed to categorise the flow patterns into four main classes: stratified flow, intermittent flow, annular flow and bubble flow. Each main class could be subdivided into subclasses. Table 1 lists the typical descriptions for two-phase flow patterns in normal and small tubes. Comparing with normal size tubes, stratified smooth flow is hardly observed in small channels whilst confined bubble flow emerges gradually due to the enhanced effect of surface tension. There is also a problematic region near intermittent and annular flow in small tubes. In this region the flow can be observed as either wavy annular (Barnea et al. [5] and Colemen and Garimella [11]) or pseudo slug (Damianides and Westwater [12]), depending on the observers.

Table 1. Classification and description of flow patterns

Main class	Subclass for normal tubes	Subclass for small tubes
Stratified flow	Stratified smooth	Stratified wavy
	Stratified wavy	
Bubble flow	Bubbly	Bubbly
	Dispersed bubble	Dispersed bubble
Intermittent flow	Plug (Elongated Bubble)	Plug (Confined Bubble)
	Slug (Taylor Bubble)	Slug (Taylor Bubble)
	Churn	Churn
		Pseudo-slug (Wavy Annular)
Annular flow	Annular	Annular
	Mist	Mist

	Wispy annular	

Some researchers thought that the models or empirical maps deduced from normal size tubes could predict flow patterns in small tubes except few transition boundaries (Mishima and Hibiki [13], Barnea et al. [5]). On the contrary, most researchers hold an opposite opinion (Coleman and Garimella [11], Triplett et al. [9]). In addition to the above disagreement, contradictory conclusions were also reported on the effect of conduit size. For example, Daminides and Westwater [12] found that the transition boundary of dispersed bubble to intermittent shifted towards lower liquid superficial velocity as the channel dimension decreases, whilst Coleman and Garimella [11] reported that it happened at higher superficial velocity, see [10].

McQuillan and Whalley [14] investigated the effect of pressure upon flow patterns. They compared the water-steam flow pattern maps in a 10 mm vertical tube at different pressures (34.5 and 69.0 MPa) and found that the slug-churn and churn-annular boundaries shift slightly towards the region of lower vapour flow rate when the pressure increases.

In this study, accurate flow visualization experiments on adiabatic R134a flow patterns in small tubes were carried out. The experimental results for the 2.01 and 4.26 mm tubes are included in reference [10]. The current completed experimental data cover four sizes tubes (1.10, 2.01, 2.88 and 4.26 mm) at three different pressures (6, 10 and 14 bar). The main objectives include: (i) obtain flow pattern maps, (ii) identify the critical diameter at the current experimental conditions, (iii) compare of flow patterns with existing models, (iv) verify the effect of the fluid pressure and diameter on flow patterns and (v) assess reference coordinate groups.

EXPERIMENTAL FACILTY

The experimental facility comprises three parts, i.e. the R22 cooling system, the R134a experimental system, see Figure 1 and the control and data acquisition system. The facility is made of stainless steel, which is also suitable for a wide range of fluids. The tested R134a liquid and vapour superficial velocity can reach 5 m/s and 10 m/s respectively. Details of the experimental system can be found in [10]. All typical flow patterns, including bubbly, dispersed bubble, confined bubble, slug, churn, annular and mist flow, were observed in the present experiments.

Four test sections, see Figure 2, with internal diameter of 1.10, 2.01, 2.88 and 4.26 mm were examined. A test section is composed of a calming section, a heating section and an observation section. Fully-developed single-phase liquid flow is formed in the calming section. Two-phase flow is created by supplying electric current directly onto the thin-wall steal tube – the heating section. The observation section, a Pyrex glass tube with the same inner diameter as the steel heating tube, is directly connected to the outlet of the heating section. Flow patterns were observed and recorded by a high-speed digital camera (Phantom V4 B/W, 512x512 pixels resolution, 1000 pictures/second with full resolution and maximum 32000 pictures/second with reduced resolution, minimum 10 microseconds exposure time).

The vital measurements in the flow pattern experiments are the temperatures (T3), the pressures (P3, P4, P0), the flow rate (F1 or F2) and the heating power (DPM2) in the test section, see Figures 1 and 2. The thermocouple T3 uses the water triple point as a reference so as to improve the measuring accuracy. The system pressure is controlled through a heater in the refrigerant tank. The heater power is automatically adjusted by a PID controller based on the signal of the pressure at the exit of the observation section (P0).

Table 2. Summary of the key parameters uncertainties

Items		Parameter	Uncertainty
Stainless Steel Tube	1.10 mm		1.31%
	2.01 mm		0.59%
	2.88 mm		0.38%
	4.26 mm		0.26%
Glass Tube	1.10 mm		0.36%
	2.01 mm		0.17%
	2.88 mm		0.06%
	4.26 mm		0.11%
Pressure	P3	6 - 14 bar	0.42%
	P4	6 - 14 bar	0.26%
	P0	6 - 14 bar	0.26%
Temperature	T3	20 - 55 ^{o}C	0.16 K
Flow Rate	CMF010	0.5 - 25 kg/hr	0.15 - 0.54%
	CMF025	25 - 500 kg/hr	0.15 - 0.22%
Heating Power	DPM2	2.68 - 1640 W	0.10 - 0.49 %
Gas Superficial Velocity	1.10 mm	0.01 - 10 m/s	0.01 - 0.41 m/s
	2.01 mm	0.01 - 10 m/s	0.01 - 0.34 m/s
	2.88 mm	0.01 - 10 m/s	0.00 - 0.32 m/s
	4.26 mm	0.01 - 10 m/s	0.00 - 0.32 m/s
Liquid Superficial Velocity	1.10 mm	0.04 - 5 m/s	0.00 - 0.15 m/s
	2.01 mm	0.04 - 5 m/s	0.00 - 0.07 m/s
	2.88 mm	0.04 - 5 m/s	0.00 - 0.05 m/s
	4.26 mm	0.04 - 5 m/s	0.00 - 0.03 m/s

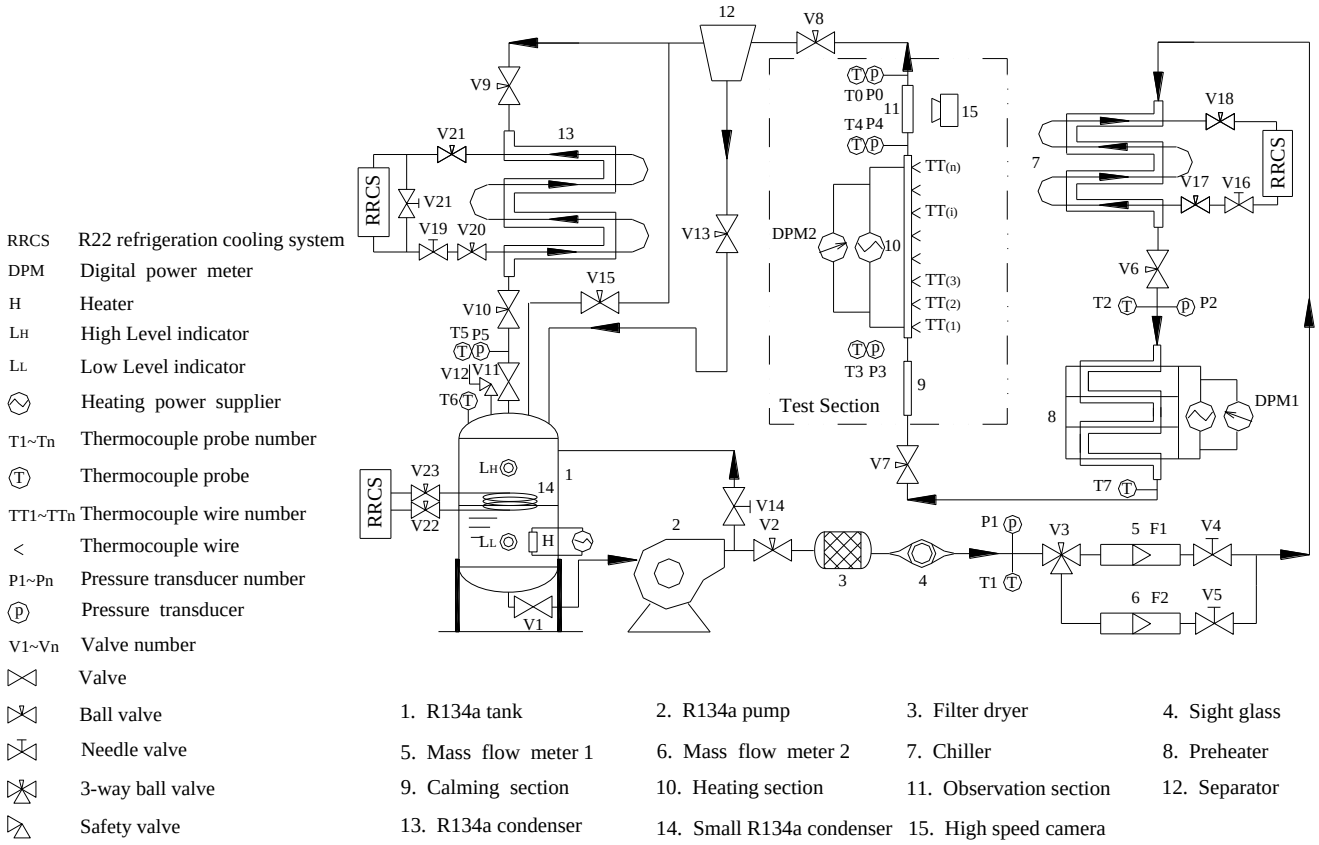

Figure 1. Schematic diagram of the flow patterns experimental facility (the R22 plant is not shown).

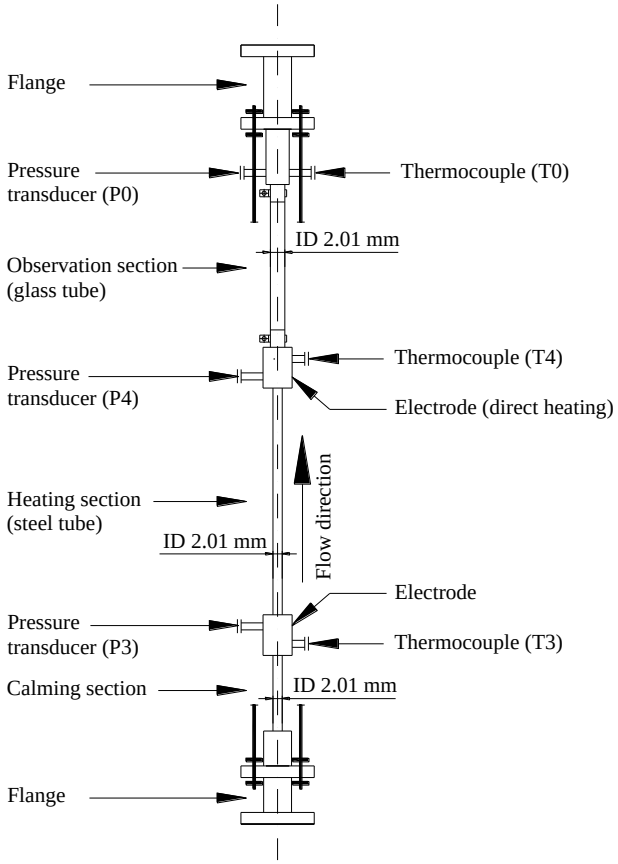

Figure 2. Schematic diagram of the 2.01 mm test section.

All the instruments were carefully calibrated. Table 2 summarizes the uncertainty in the key parameters of the current experiments. The overall system performance was validated through single-phase experiments, e.g. the turbulent experimental friction factor agreed with the Blasius equation within ± 5 % over the Reynolds range of 4000 to 110000. The experimental parameters at the observation point in the two-phase flow patterns experiments were deduced from the inlet and outlet saturated pressure and the assumption that the pressure drop along the observation section was linear. The liquid and vapour superficial velocities were varied and calculated for each diameter and pressure by changing the flow rate and heating power, see [10]. The number of data points obtained near the transition boundaries was higher than at other conditions in order to get more details at that zone.

EXPERIMENTAL RESULTS

Dispersed bubble, bubbly, slug, churn and annular flow were observed in all four test sections. Occasionally mist flow was observed at very high vapour velocity whilst confined bubble flow was found at lower vapour and liquid velocity. The above-mentioned seven flow patterns are defined as follows:

Dispersed bubble: numerous small bubbles float in a continuous liquid phase.

Bubbly: bubble size is comparable to but not as large as the tube diameter.

Confined bubble: bubble sizes reach the diameter of the tube and are confined by the tube wall. They have regular vapour-liquid interface and spherical cap and bottom.

Slug: bubbles develop into bullet shape due to the tube wall restriction. Sometimes the bullet bubbles are followed by a stream of small bubbles creating a trail.

Churn: bullet bubbles start to distort and small bubbles in liquid slug coalesce into gas clump with increase of gas velocity. It is a highly oscillatory flow with chaotic interface.

Annular: gas phase becomes a continuous flow in the core of the tube.

Mist: liquid film is blown away from tube wall and numerous liquid droplets float in high-speed vapour flow.

Figures 3-6 show the above flow patterns obtained by the digital high-speed camera in the 1.10, 2.01, 2.88 and 4.26 mm diameter tubes at 10 bar pressure. The flow patterns in 2.01 and 4.26 were first reported in [10] but are included here for completeness. Overall the flow patterns in the four tubes are similar and could be grouped into the above seven typical patterns – note that mist flow was obtained in the 4.26 mm tube only. Annular–mist transition flow was observed in the 2.01 and 2.88 mm tubes, i.e. liquid film sticks on the tube wall whilst the liquid droplets pass through intermittently. This discontinuous liquid droplet flow may be the result of the collapse of liquid slug in churn flow in the heating section. The high velocity vapour current breaks up the liquid blocks and creates numerous liquid droplets. After that, the experiments were stopped before reaching critical heat flux. The 1.10 mm tube was not tested under very high fluid velocity because the resulting excessive pressure drop can cause system unsteadiness. Similar results were obtained at the pressures of 6 and 14 bar. As stated above, all the flow patterns for the four tubes observed in the experiments were of the typical categories mentioned above. However, on closer observations, there are some differences among these tubes. Confined bubble flow, a special slug flow with elongated spherical top and bottom bubbles, was only observed in the 1.10 mm tube at the 6.0 to 14.0 bar and 2.01mm tube at 6.0 bar. It indicates that surface tension has grown into a dominant force in the small tubes at the lower fluid velocities. With the increase of fluid velocities, as shown in Figure 3, the gas-liquid interface became irregular and chaotic. Inertial force and friction gradually take the place of surface tension to become the important factors in flow pattern transitions.

The flow patterns in the 2.88 and 4.26 mm tube do not exhibit any common characteristics of the flow patterns in small tubes. Comparatively, the flow patterns in the 2.01 mm tube showed part "small tube characteristics", which indicate the increasing action of the surface tension and the tube confinement, e.g. the slimmer plug, the thinner liquid film around the plug, and the less chaotic vapour-liquid interface in churn flow. When tube diameter decreases to 1.10 mm, the full small tube characteristics, as also described in the previous studies, are exhibited. Therefore, the 2.01 mm tube possesses both characteristics of the normal size and the small tube. From this point of view, the tube diameter around of 2.01 mm could be regarded as a critical diameter for refrigerant R134a for the current range of experimental conditions.. This result agrees with the criterion by Kew and Cornwell [7], e.g. 1.9 mm at 3 bar , [10].

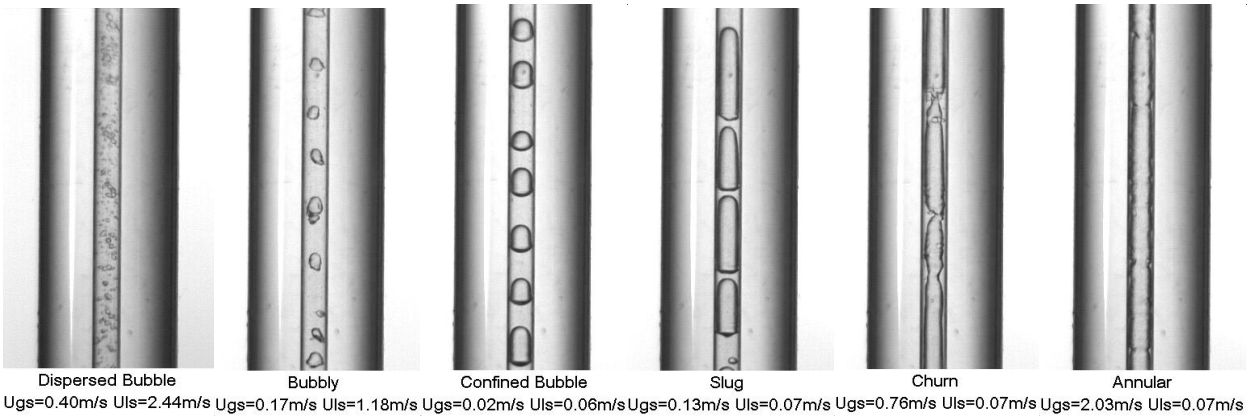

Figure 3. Flow patterns observed in the 1.10 mm internal diameter tube at 10 bar.

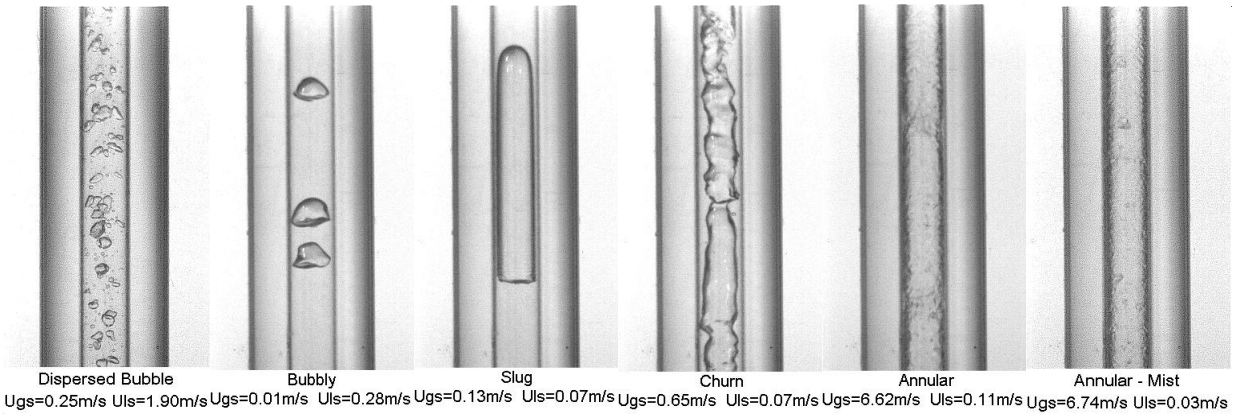

Figure 4. Flow patterns observed in the 2.01 mm internal diameter tube at 10 bar.

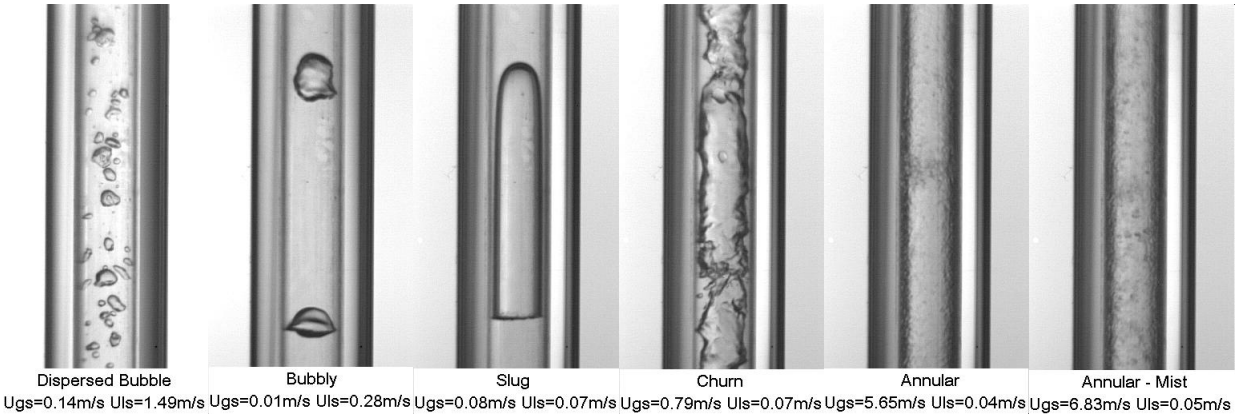

Figure 5. Flow patterns observed in the 2.88 mm internal diameter tube at 10 bar.

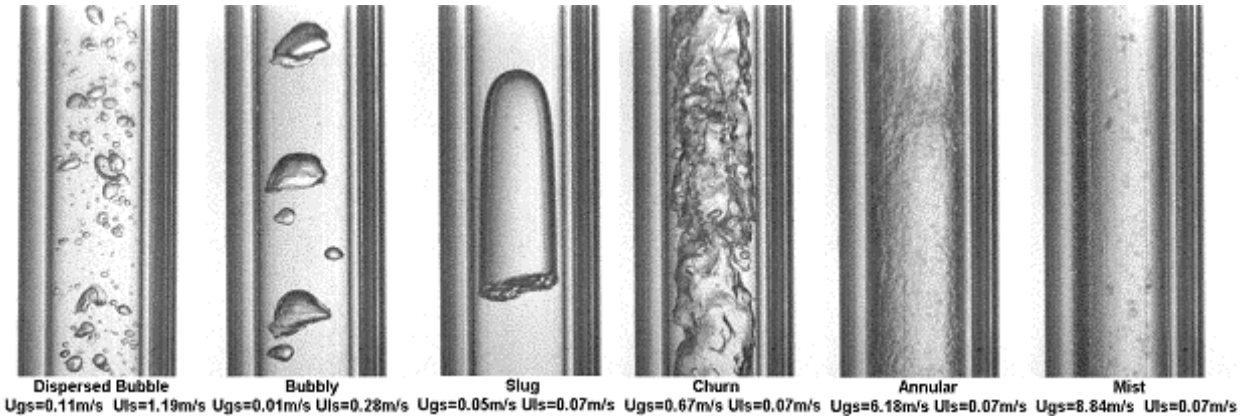

Figure 6. Flow patterns observed in the 4.26 mm internal diameter tube at 10 bar.

Twelve flow pattern maps were generated based on all the results obtained for the 1.10, 2.01, 2.88 and 4.26 mm tubes at 6, 10 and 14 bar pressure. The flow pattern maps for the 2.01 and 4.26 mm tubes were compared with the existing models for vertical upward flow in normal size tubes and showed poor agreement in Chen et al. [10]. The models included the unified model summarized by Taitel [15] and the models given by Taitel et al. [16], Mishima and Ishii [17] and McQuilian and Whalley [14]. Figures 7-10 depict a comparison of the flow maps for 1.10-4.26 mm tubes with the unified model summarized by Taitel [15]. As expected, the newly obtained flow maps for the 1.10 and 2.88 mm tubes cannot be predicted by these models and the discrepancy is higher in the smaller tubes. For example, the shaded region in which the predicted annular flow falls into the region of slug flow increases and the transition boundary of dispersed bubble to slug flow differs more from the predictions.

The recently obtained data for the 1.10 and 2.88 mm test sections also support the existing conclusions deduced for the 2.01 and 4.26 mm tubes about the effect of pressure and diameter on flow patterns. As seen in figures 11-12 (the data for 2.01 and 4.26 mm tubes are omitted here since they appear in [10]) the transition boundaries of slug-churn and churn-annular flow shift slightly towards the region of lower vapour flow rate when the pressure increases, i.e. the same observation as McQuillan and Whalley [14]. The dispersed bubble-bubbly, dispersed bubble-churn and bubbly-slug boundaries are hardly affected by pressure in the current experiments. The possible reasons were presented in [10], i.e. the change of surface tension and vapour density. The effect of diameter on flow patterns is depicted in Figures 13-15. Reducing the diameter shifts the transition boundaries of slug-churn and churn-annular to higher values of vapour velocity. This result is in agreement with the experiments of Coleman and Garimella [11] and Daminides and Westwater [12] but contrary to the results of Lin et al. [6]. Also, the dispersed bubble-bubbly boundary shifts to higher liquid velocity with a reduction in the diameter. There seems to be no change for these four diameters at the boundary between dispersed bubble – churn and bubbly-slug flow.

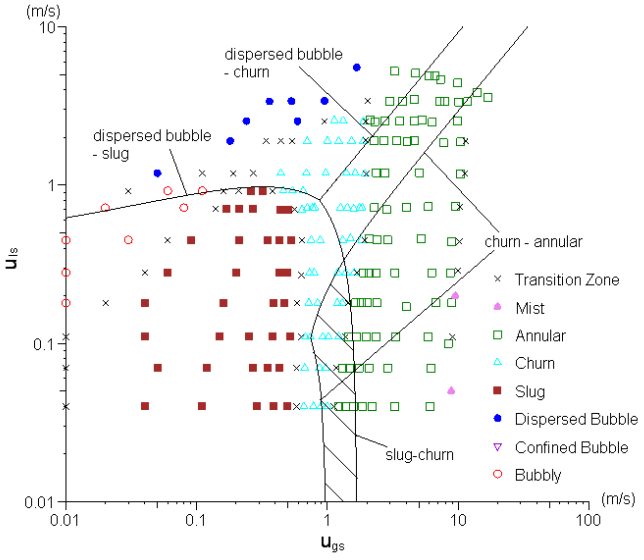

Figure 7. Flow pattern map for R134a in the 4.26 mm tube at 10 bar and comparison with the unified model (Taitel, [15]).

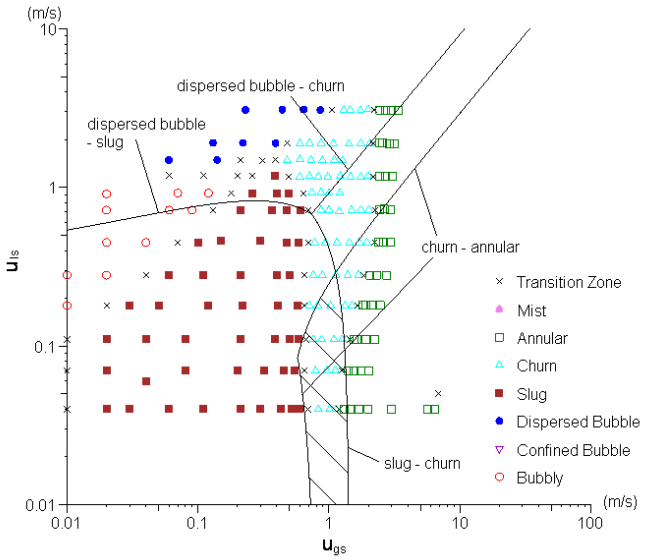

Figure 8. Flow pattern map for R134a in the 2.88 mm tube at 10 bar and comparison with the unified model (Taitel, [15]).

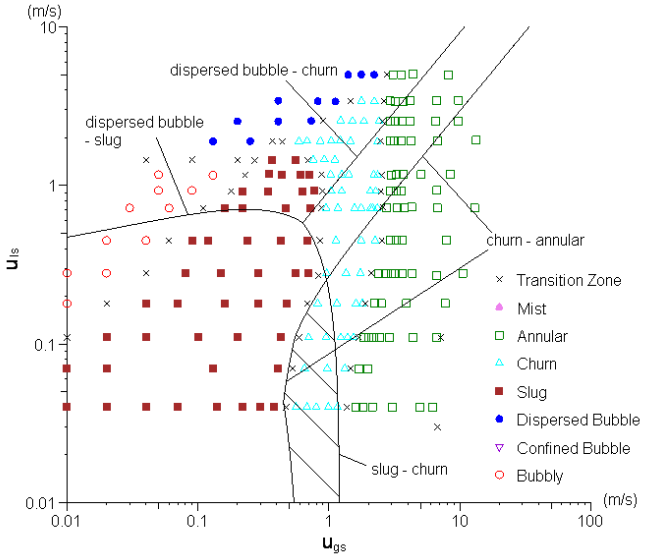

Figure 9. Flow pattern map for R134a in the 2.01 mm tube at 10 bar and comparison with the unified model (Taitel, [15]).

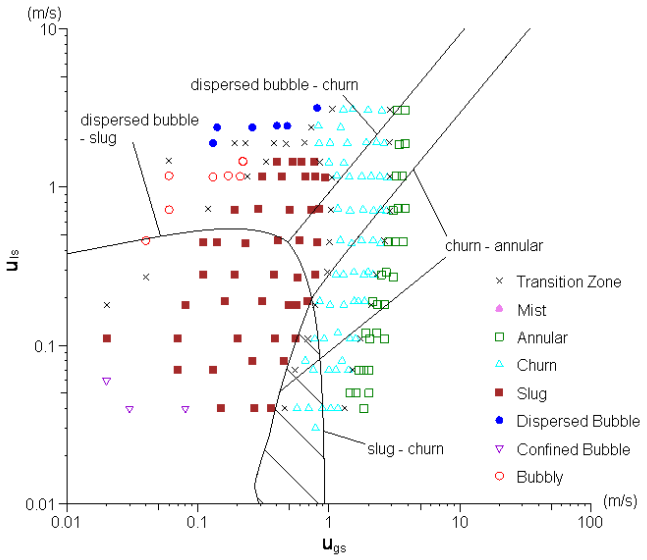

Figure 10. Flow pattern map for R134a in the 1.10 mm tube at 10 bar and comparison with the unified model (Taitel, [15]).

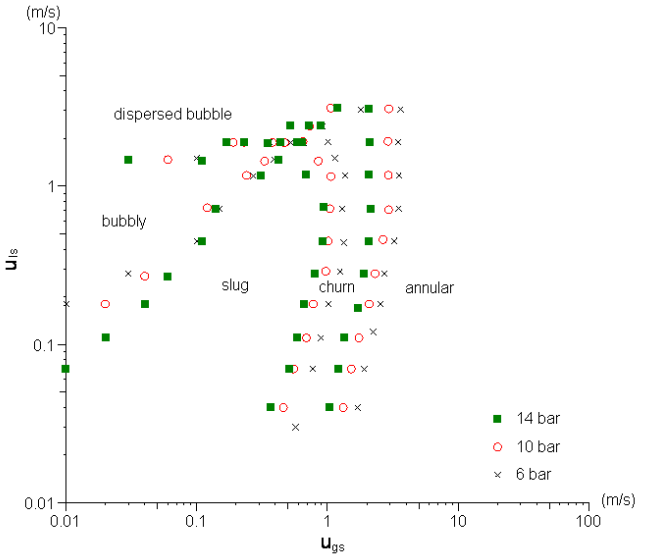

Figure 11. Effect of pressure on transition boundaries for the 1.10 mm tube.

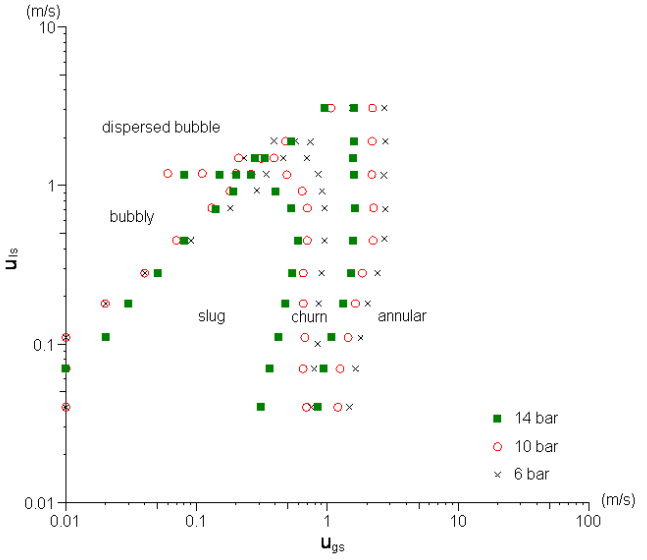

Figure 12. Effect of pressure on transition boundaries for the 2.88 mm tube.

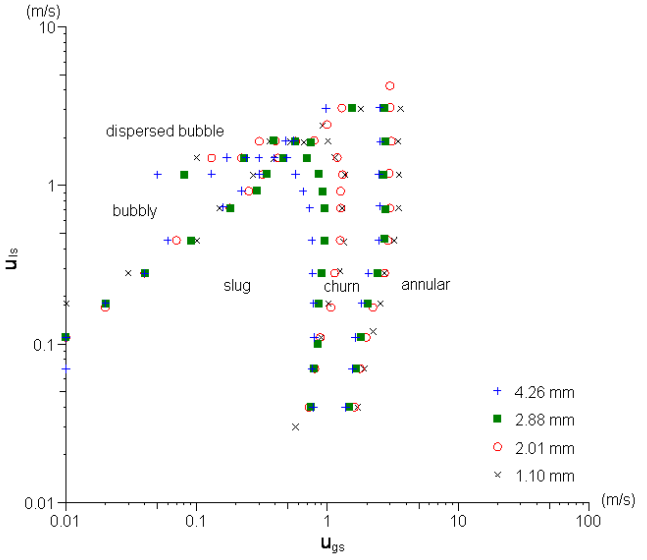

Figure 13. Effect of diameter on transition boundaries at 6 bar.

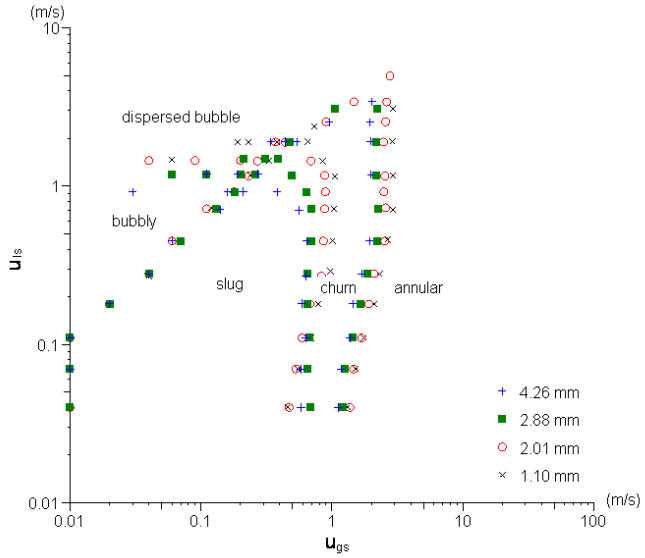

Figure 14. Effect of diameter on transition boundaries at 10 bar.

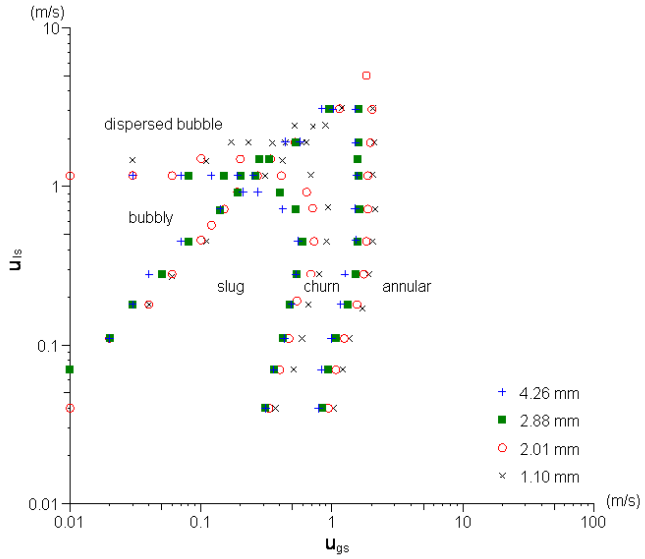

Figure 15. Effect of diameter on transition boundaries at 14 bar.

The above flow maps were sketched using the superficial velocities as coordinates. Flow maps were also plotted using different coordinate systems in an attempt to obtain general and accurate prediction of the patterns in earlier studies. The dimensionless coordinate groups were regarded to be more general and effective since these can contain a group of parameters. However, no one coordinate group was widely accepted among the researchers yet. The present study examined the experimental data with a number of coordinate groups which are listed below:

(1) u_{gs} vs. u_{ls}

(2) x vs. G

(3) $\left(\frac{\upsilon_{gref}}{\upsilon_g}\right)^{1/3}\left(\frac{\upsilon_{lref}\,\sigma_{ref}}{\upsilon_l\,\sigma}\right)^{1/4} u_{gs}$ vs. $\left(\frac{\upsilon_{lref}\,\sigma_{ref}}{\upsilon_l\,\sigma}\right)^{1/4} u_{ls}$

(4) G_{gs}/λ vs. $G_{ls}\psi$

$$\lambda = \sqrt{\frac{\rho_g \rho_l}{\rho_{gref}\rho_{lref}}} \qquad \psi = \frac{\sigma_{ref}}{\sigma}\left[\frac{\mu_l}{\mu_{lref}}\left(\frac{\rho_{lref}}{\rho_l}\right)^2\right]^{1/3}$$

(5) $\frac{G_{ls}}{G_{gs}}\lambda\psi$ vs. $\frac{G_{gs}}{\lambda}$

(6) u_h vs. β

(7) G_{gs} vs. G_{ls}

(8) Fr_h vs. β

(9) $u_{gs}^2\rho_g$ vs. $u_{ls}^2\rho_l$

(10) $\frac{u_{gs}}{u_{ls}}$ vs. u_{ls}

(11) $\dot{m}_l$ vs. $\dot{m}_g$

(12) Re_{gs} vs. Re_{ls}

(13) We_{gs} vs. We_{ls}

(14) X vs. Y

$$Y = \frac{(\rho_l - \rho_g)g}{\Delta P_g}$$

(15) $u_{gs}\sqrt{\frac{\rho_g}{gD(\rho_l-\rho_g)}}$ vs. $u_{ls}\sqrt{\frac{\rho_l}{gD(\rho_l-\rho_g)}}$

(16) $u_{gs}\sqrt{\frac{\rho_g}{\sqrt{g\sigma(\rho_l-\rho_g)}}}$ vs. $u_{ls}\sqrt{\frac{\rho_l}{\sqrt{g\sigma(\rho_l-\rho_g)}}}$

(17) $\frac{u_{gs}}{D}\sqrt{\frac{\rho_g}{\sqrt{g\sigma(\rho_l-\rho_g)}}}\sqrt{\frac{\sigma}{g(\rho_l-\rho_g)}}$

vs.

$\frac{u_{ls}}{D}\sqrt{\frac{\rho_l}{\sqrt{g\sigma(\rho_l-\rho_g)}}}\sqrt{\frac{\sigma}{g(\rho_l-\rho_g)}}$

(18) $u_{gs}\left(\frac{\rho_g}{g\sigma}\right)^{0.25}$ vs. $u_{ls}\left(\frac{\rho_l}{g\sigma}\right)^{0.25}$

The flow maps based on the above coordinate groups seems disorderly without following an obvious rule. However, the group of Lockhard-Martinelli parameter and mass flux, X vs. G, apparently include the effect of fluid pressure on the transition boundaries of slug to churn and churn to annular, see Figures 16-19. They might be the suitable parameters to predict slug, churn and annular flow. A possible reason may be that friction is a prevailing force in these two transition boundaries. The Lockhard-Martinelli parameter quantitatively presents the friction ratio between the gas and liquid phases and mass flow flux is directly related to the overall fluid friction. However, this needs further study and validation.

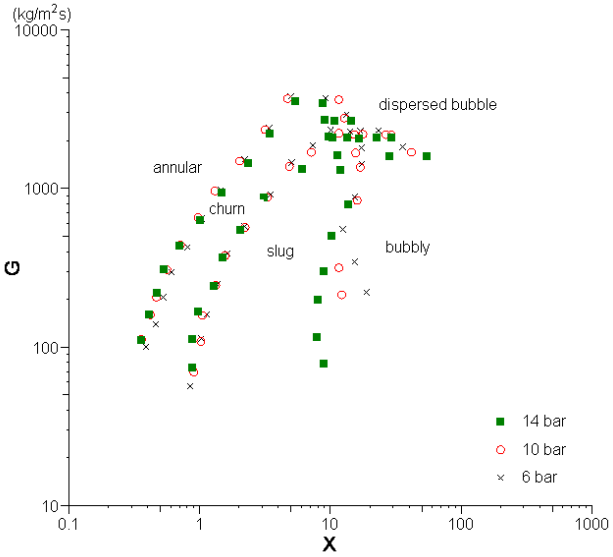

Figure 16. Comparison of the flow pattern transition boundaries using the Lockhard-Martinelli Parameter and mass flux for the 1.10 mm tube.

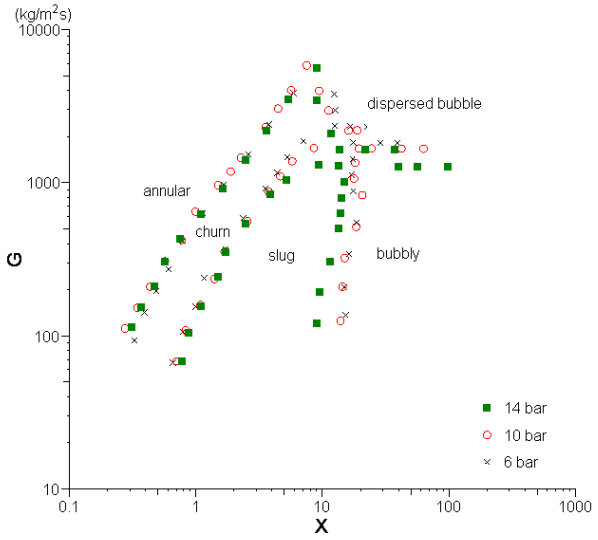

Figure 17. Comparison of the flow pattern transition boundaries using the Lockhard-Martinelli Parameter and mass flux for the 2.01 mm tube.

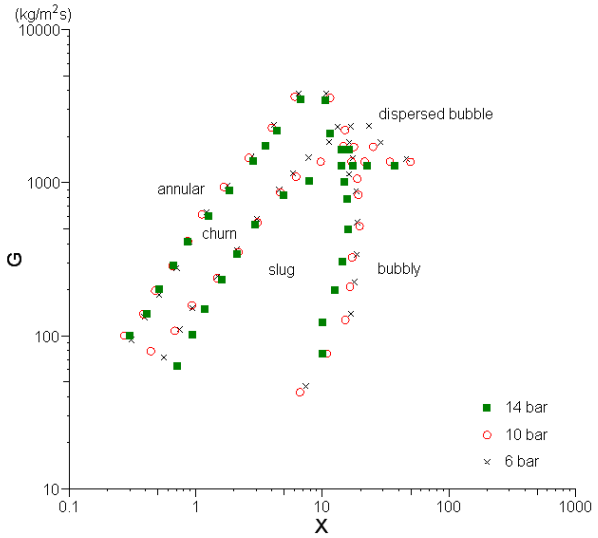

Figure 18. Comparison of the flow pattern transition boundaries using the Lockhard-Martinelli Parameter and mass flux for the 2.88 mm tube.

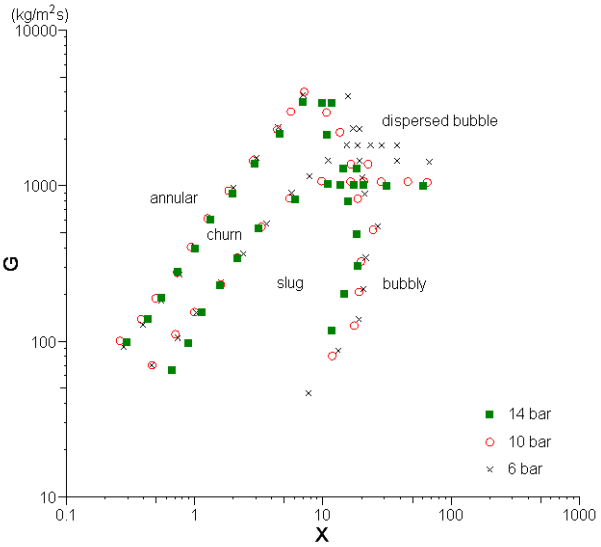

Figure 19. Comparison of the flow pattern transition boundaries using the Lockhard-Martinelli Parameter and mass flux for the 4.26 mm tube.

CONCLUSIONS

Seven typical flow patterns were observed for the present experimental conditions, i.e. dispersed bubble, bubbly, confined bubble, slug, churn, annular and mist. The experimental results indicate that the flow patterns for the larger diameters (2.88 and 4.26 mm) exhibit strong characteristics of normal size tubes. When the tube diameter was reduced to 2.01 mm, the flow patterns exhibit the "small tube characteristics" until the confined bubble flow appears in the 1.10 mm tube which indicates that surface tension become the dominant force. The critical diameter used to distinguish small and normal pipe could be deduced from the above observations, is about 2 mm for the current experimental conditions. Twelve flow pattern maps were drawn and compared with the existing models for normal size tubes indicating significant differences in the 4.26 mm tube and more so for the smaller tubes. The boundaries of slug to churn and churn to annular moved to higher vapour velocity when the diameter changed from 4.26 to 1.10 mm; the dispersed bubble to bubbly boundary moved to higher liquid velocity. The diameter does not seem to affect the dispersed bubble to churn and bubbly to slug. When the pressure increases the boundaries of slug to churn and churn to annular moved to lower vapour velocity. No or little effect was observed on the dispersed bubble to bubbly, dispersed bubble to churn and bubbly to slug boundaries with pressure changes. The current research and experimental data indicates that the coordinate group of the Lockhard-Martinelli Parameter and mass flux may be the right parameters to deduced general correlations to predict the transition boundaries of slug to churn flow or churn to annular flow.

NOMENCLATURE

Co	Confinement number, $\left[\sigma / D^2 g (\rho_l - \rho_g)\right]^{1/2}$
D	tube diameter, m
Eö	Eotvös number, $[(2\pi)^2 \mathrm{Co}^2]$
Fr	Froude number, $[u^2/gD]$
G	mass flux, kg/m^2s
g	gravitational acceleration, m/s^2
$\dot{m}$	mass flow rate, kg/s
ΔP	pressure drop, Pa
Re	Reynold number, $[GD/\mu]$
u	velocity, m/s
We	Weber number, $\rho u^2 D/\sigma$
X	Lockhart-Martinelli parameter, $[(\Delta p_{ls}/\Delta p_{gs})^{1/2}]$
x	quality

Greeks symbols

β	volume flow ratio, $[x\rho_l / (\rho_l + (-x)\rho_g)]$
μ	dynamic viscosity, kg/m s
ρ	density, kg/m^3
σ	surface tension, N/m
υ	specific volume, m^3/kg

Subscripts

g	saturated gas/vapour
gs	based on superficial gas velocity
h	homogeneous
l	saturated liquid
ls	based on superficial liquid velocity
ref	reference fluid

REFERENCES

1. T. Fukano and A. Kariyasaki, Characteristics of gas-liquid two-phase flow in a capillary tube, Nuclear Engineering and Design, Vol. 141, pp. 59-68, 1993.
2. D.C. Zietlow and C.O. Pedersen, Flow regime mapping and analysis of R-134a in a small-channel cross-flow condenser, ASHRAE Transactions, Vol. 104, No. 2, pp. 540-547, 1998.
3. S. Wongwises, S. Disawas, J. Kaewon and C. Onurai, Two-phase evaporative heat transfer coefficients of refrigerant HFC-134a under forced flow conditions in a small horizontal tube, Int. Comm. Heat Mass Transfer, Vol. 27, No. 1, pp. 35-48, 2000.

4. T. Oya, Upward liquid Flow in small tube into which air streams (1st Report, Experimental apparatus and flow patterns), Vol. 14, No. 78, pp. 1320-1329, 1971.
5. D. Barnea, Y. Luninski and Y. Taitel, Flow pattern in horizontal and vertical two phase flow in small diameter pipes, The Canadian Journal of Chemical Engineering, Vol. 61, No. 5, pp. 617-620, 1983.
6. S. Lin, P.A. Kew and K. Cornwell, Two-phase flow regimes and heat transfer in small tubes and channels, Heat Transfer1998, Proceedings of 11th IHTC, Vol. 2, August 23-28, Kyongju, Korea, pp. 45-50, 1998.
7. P.A. Kew and K. Cornwell, Correlations for the prediction of boiling heat transfer in small-diameter channels, Applied Thermal Engineering, Vol.17, Nos.8-10, pp.705-715, 1997.
8. N. Brauner and D. Moalem-Maron, Identification of the range of small diameter conduits, regarding two-phase flow pattern transitions, Int. Commun. Heat Mass Transfer, Vol. 19, pp. 29-39, 1992.
9. K. A. Triplett, S.M. Ghiaasiaan, S.I. Abdel-Khalik and D.L. Sadowski, Gas-liquid two-phase flow in microchannels, Part I: Two-phase flow patterns, International Journal of Multiphase Flow, Vol. 25, Elsevier Science Ltd., pp. 377-394, 1999.
10. L. Chen, Y. S. Tian and T. G. Karayiannis, R134a Flow Patterns in Small Diameter Tubes, In press, Journal of Process Mechanical Engineering, Proc. Of the Inst. of Mechanical Engineers, Part E.
11. J.W. Coleman and S. Garimella, Characterization of two-phase flow patterns in small diameter round and rectangular tubes, International Journal of Heat and Mass Transfer, Vol. 42, pp. 2869-2881, 1999.
12. D.A. Damianides and J.W. Westwater, Two-phase flow patterns in a compact heat exchanger and in small tubes, Second UK National Conference on Heat Transfer, Volume 11 Sessions 4A-6C, pp. 1257-1268, 1988.
13. K. Mishima and T. Hibiki, Some characteristics of air-water two-phase flow in small diameter vertical tubes, Int. J. Multiphase flow, Vol. 22, No. 4, pp. 703-712, 1996.
14. K. W. McQuillan and P. B. Whalley, Flow patterns in vertical two-phase flow, Int. J. Multiphase Flow, Vol. 11, No. 2, pp. 161-175, 1985.
15. Y. Taitel, Flow pattern transition in two phase flow, Keynote lecture, 9th International Heat Transfer Conference, Jerusalem, Israel, 19-24 Aug., pp. 237-254, 1990.
16. Y. Taitel, D. Barnea and A. E. Dukler, Modelling flow pattern transitions for steady upward gas-liquid flow in vertical tubes, AIChE, Vol. 26, pp. 345-354, 1980.
17. K. Mishima and M. Ishii, Flow regime transition criteria for upward two-phase flow in vertical tubes, Int. J. Heat Mass Transfer, Vol. 27, No. 5, pp. 723-737, 1984.